International Journal of Nanoelectronics and Materials
Volume 13, No. 2, Apr 2020 [307-314]

All-Solution-Non-Vacuum Fabrication Process of CZTS Solar Cell using ZTO as Non-Toxic Buffer Layer

Yusuf Yuda Prawira[1], Eka Cahya Prima[2], Gema Refantero[1], Harbi Setyo Nugroho[1], Christian Harito[1,4,5], Rachmat Adhi Wibowo[3], Nugraha[1,5], Camelia Panatarani[6] and Brian Yuliarto[1,5*]

[1]*Advanced Functional Materials (AFM) Laboratory, Engineering Physics, Institut Teknologi Bandung, 40132, Bandung, Indonesia.*
[2]*Department of Science Education, Faculty of Mathematics and Science Education, Universitas Pendidikan Indonesia, 40154, Bandung, Indonesia.*
[3]*AIT Austrian Institute of Technology, Center for Energy, Photovoltaic Systems, Giefinggasse 6, A-1210 Vienna, Austria.*
[4]*Energy Technology Research Group, Faculty of Engineering and Physical Sciences, University of Southampton, SO17 1BJ, Southampton, U.K.*
[5]*Research Center for Nanosciences and Nanotechnology (RCNN), Institut Teknologi Bandung, 40132, Bandung, Indonesia.*
[6]*Department of Physics, Faculty of Mathematics and Natural Science, Universitas Padjadjaran, 45363, Sumedang, Indonesia.*

Received 25 October 2019, Revised 10 January 2020, Accepted 30 January 2020

ABSTRACT

Material based on copper zinc tin sulfide (CZTS) has been investigated to obtain its optimum performances due to the non-toxicity, elemental abundance, and large production capacity. In this work, fabrication of CZTS-based thin-film solar cells was carried out using an all-solution-non-vacuum-based method and spin-coating process for layer deposition. Additionally, the ZTO buffer layer was used as an alternative buffer layer instead of other materials such as CdS. The bandgap energies of the CZTS absorber layer and ZTO buffer layers are ~1.5 eV and ~3.7 eV, respectively. The solar cell fabricated by the all-solution process using the ZTO buffer layer exhibited the power conversion efficiency of 0.28%.

Keywords: Solar Cell, CZTS, ZTO, All-Solution-Non-Vacuum Process.

1. INTRODUCTION

Cu_2ZnSnS_4 (CZTS) is one of the promising alternative materials for the absorber layer of thin-film solar cells due to the non-toxicity, elemental abundance, and large production capacity [1], [2]. Moreover, CZTS-based material has a direct bandgap of ~1.5 eV and a high absorption coefficient ($\alpha > 10^4$ cm^{-1}) [3]. Henceforth, CZTS-based thin-film solar cell has been investigated thoroughly by many researchers in order to obtain its optimum performances [4]–[8]. As for now, the highest efficiency among CZTS-based thin-film solar cell is 12.6% [9].

So far, several methods have been used to deposit the CZTS absorber layer on the Mo-coated soda-lime glass substrate such as sputtering, atomic layer deposition, chemical bath deposition, thermal evaporation, spin-coating, electro-deposition, hydrazine slurry method, and spray pyrolysis method [9]–[13]. Chemical bath deposition is commonly used to deposit the buffer

*Corresponding Author: *berayen@gmail.com*

layer on top of the absorber layer and then sputtering is used to deposit transparent conductive oxide [14]–[16].

Different from the previous works, all-non-vacuum spin-coating based on the non-toxic solution process was applied to fabricate the CZTS-based thin-film solar cell. This method offers a lower fabrication cost and a safer production method compared to other fabrication processes such as sputtering, hydrazine slurry method, and spray pyrolysis method. In this study, different buffer layer material was also used, namely ZTO (Zinc-Tin-Oxide). Compared to the CdS based buffer layer, the ZTO-based buffer layer is a safer choice since ZTO is a non-toxic material [17]. Besides, ZTO material is cheaper and more elemental abundant than CdS material [17].

2. DEVICE FABRICATION

The CZTS precursor solution contained 0.52 M $Cu(CH_3COO)_2.H_2O$, 0.33 M $Zn(CH_3COO)_2.2H_2O$, 0.27 M $SnCl_2.2H_2O$, and 2.06 M CH_4N_2S that were dissolved at 60°C for 2 hours. The CZTS precursor solution was spin-coated onto Mo-coated soda-lime glass and then dried on a hotplate at 280°C for 2 minutes. The spin-coating process was done at 3000 rpm for 30 seconds. The samples were then sulfurized at 580°C for 2 hours. No etchants treatment was applied after sulfurization. The ZTO precursor solution consisted of $Zn(CH_3COO)_3.H_2O$ and $SnCl_2.2H_2O$ were dissolved in 2-methoxyethanol. Different compositions of ZTO were labelled as A, B, C, and D with different Zn:Sn ratio of 1:19, 3:7, 1:1, and 7:3, respectively. ZTO buffer layer deposited above the CZTS absorber layer using the spin-coating process at 3000 rpm for 30 seconds and dried at 95°C for 2 minutes. The spin-coating and drying steps were repeated differently to observe the amount of repetition which yields ZTO thickness of 50 – 60 nm. The devices were then completed also using the spin-coating process to deposit the AZO layer with a thickness of 350 – 400 nm. Finally, a silver paste was used to print the top electrode.

3. RESULTS AND DISCUSSIONS

3.1 Characterization of CZTS Absorber Layer

The architecture design of CZTS solar cell and the cross-section of CZTS absorber was captured using a Scanning Electron Microscope (SEM) as shown in Figures 1 and 2, respectively. The sulfurization of the sample was done under N_2, atmosphere at 580°C for 2 hours. After sulfurization, the CZTS absorber layer with a thickness of ~0.8 μm was obtained. The existence of the ZnS secondary phase was found at the surface of the CZTS absorber, resulting in a total thickness of ~1.3 μm. The SEM cross-sectional image also shows that the majority of the CZTS absorber layer consists of small grain. The formation of small grain was due to the instability of CZTS absorber under high-temperature annealing [18]. This small grain induces large grain boundaries within the absorber layer which relates to their associated structural defect [19].

Figure 3 shows the X-ray Diffraction (XRD) pattern of the CZTS absorber layer. Based on the comparison of the sample XRD pattern with Crystallography Open Database (COD) reference (ID: 96-900-4751), the peaks of XRD pattern at 28.46°, 47.31°, and 56.41° which were indexed as (112), (204), and (312) planes, respectively, where all belong to CZTS kesterite crystal structure. The primary orientation of the CZTS kesterite crystal structure is (112) plane as it showed the highest intensity among other orientations. The kesterite crystal structure was successfully grown from amorphous CZT after sulfurization as shown in Figure 3. The blue line belongs to the sample pre-sulfurization XRD pattern, whereas the red line belongs to the sample post-sulfurization XRD pattern. As previously mentioned, the presence of the ZnS secondary phase was also observed at the XRD pattern near the kesterite (112) peak.

The Tauc plot characteristic of the CZTS absorber layer was obtained using UV-Vis characterization as shown in Figure 4. The absorption coefficient and photon energy are labelled as α and hυ, respectively. The Tauc plot can be used to harvest the bandgap energy of CZTS absorber by interpolating the linear region in the $(\alpha h\upsilon)^2$ curve to intercept the photon energy axis. The intercept point in the photon energy axis was then defined as the CZTS absorber bandgap energy. Based on this analysis, the CZTS absorber has a direct bandgap energy of ~1.5 eV. This bandgap value is a characteristic of CZTS material as an absorber layer as obtained in other references [3], [20], [21].

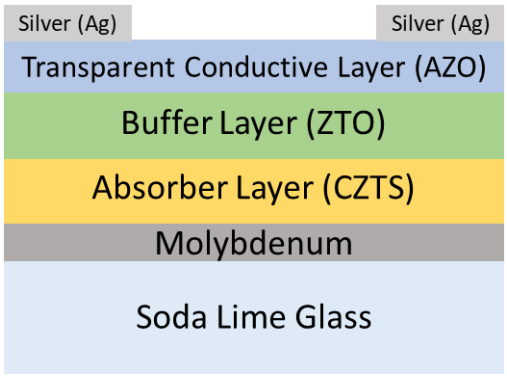

Figure 1. The architecture design of CZTS Solar cell

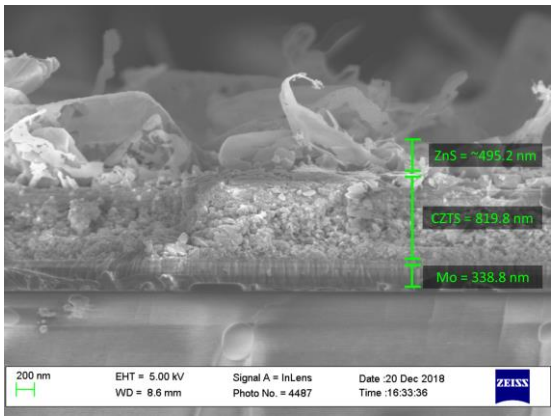

Figure 2. The SEM cross-sectional image of the CZTS absorber layer after sulphurization

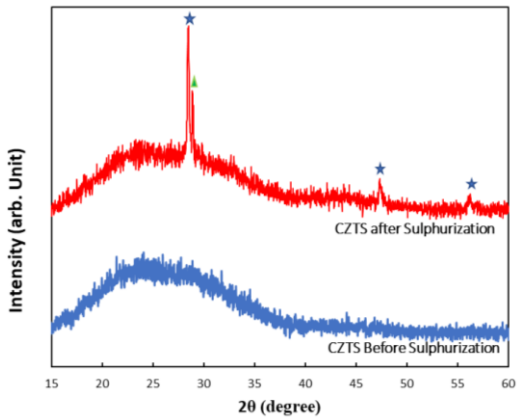

Figure 3. The XRD pattern of CZTS absorber before (blue line) and after (red line) sulfurization

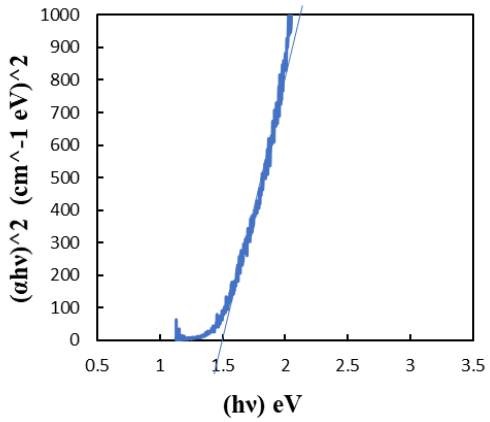

Figure 4. The Tauc plot characteristic of the CZTS absorber layer

3.2 Characterization of ZTO Buffer Layer

ZTO samples with different compositions were deposited using the spin-coating process. The deposition was done several times to obtain the optimum thickness of the buffer layer of about 50 – 60 nm [19]. Profilometer analysis was done to measure the optimum thickness of the ZTO buffer layer. Figure 5 shows the ZTO thickness profile with respect to the deposition amount. The ZTO samples were labelled as A, B, C, and D which the Zn:Sn stoichiometric ratio of each sample was 1:19, 3:7, 1:1, and 7:3. For all samples, different deposition amounts of 2, 6, 10, and 14 times were then applied. The optimum thickness of the ZTO buffer layer was obtained for all samples with deposition amounts of 6 times which has a thickness of about 50 – 60 nm.

Figure 6 shows the Tauc plot characteristic of the ZTO buffer layer with different compositions. The characterization was carried out to analyse the bandgap energy of each ZTO sample. The results show that the range of bandgap energy for each sample was around 3.7 – 3.9 eV with the

lowest bandgap energy belong to sample A (Zn:Sn=1:19). By having a bandgap of that high, the potential for electron-hole pairs to form in the absorber layer will be greater. Hence, the buffer layer suitable for the CZTS absorber layer is the band alignment formed by the two layers, which spike conformation band alignment is less detrimental than the cliff conformation one [19]. Moreover, Cui et al. (2018) and Albar et al. (2019) [22], [23] have reported that the CZTS/ZTO band alignment forms a spike conformation, which makes ZTO as a suitable buffer layer for CZTS solar cells. Further analysis to observe the semiconductor type of each sample was done using CO as a reducing gas. During reaction with CO gases, increasing resistivity occurs on the p-type semiconductor whereas decreasing resistivity occurs on the n-type semiconductor [24]. Table 1 shows the result of the semiconductor type examination of the ZTO samples. The result shows that sample A is the only one that has decreasing resistivity during its reaction with CO gases, making it the only n-type sample. Thus, only sample A can produce a photovoltaic effect when assembled with the CZTS absorber layer. Therefore, for further work, ZTO was used with Zn:Sn ratio of 1:19 (sample A) with deposition amounts of 6 times.

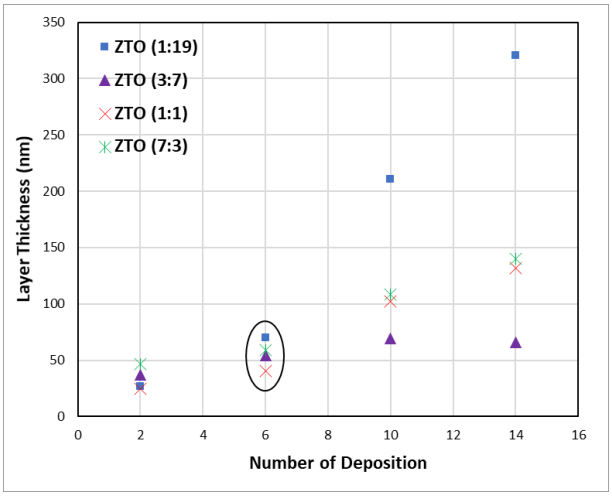

Figure 5. The thickness of the ZTO buffer layer analysed using the profilometer analysis.

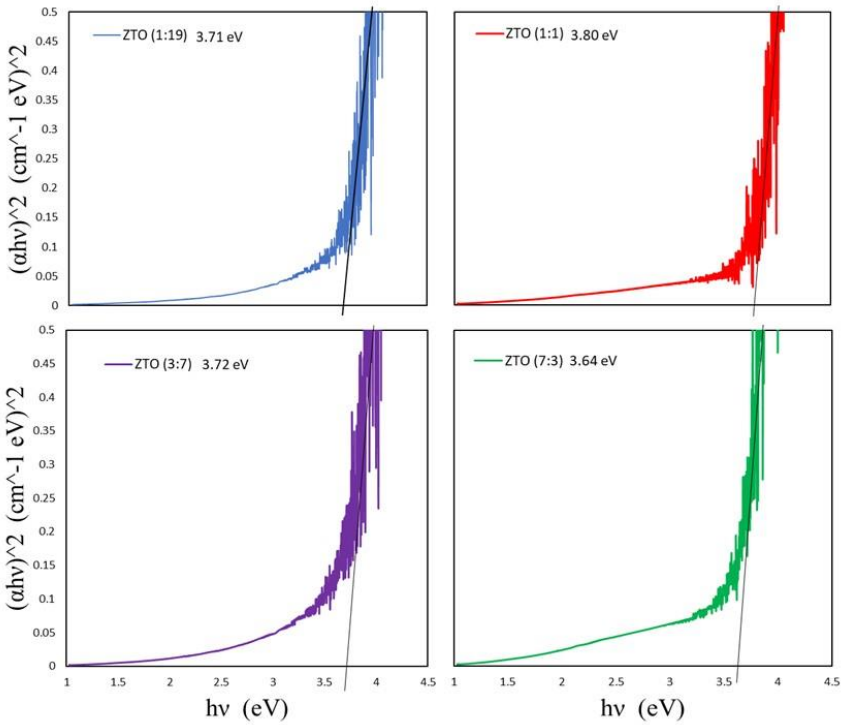

Figure 6. The Tauc plot characteristic of ZTO buffer layer with different composition.

Table 1 The semiconductor type examination of the ZTO samples

Sample	Zn:Sn Ratio	ΔR	Semiconductor Type
A	1:19	Decrease	n
B	3:7	Increase	p
C	1:1	Increase	p
D	7:3	Increase	p

3.3 Device Performance

Figure 7 shows the I-V characteristics of device A measured under dark and simulated AM 1.5 illumination. The fabricated device yields a power conversion efficiency (PCE) of 0.28% with a short circuit current (I_{sc}) of 112.52 mA and an open-circuit voltage (V_{oc}) of 0.52 V. The device fill factor (FF) of 26.75% was also obtained from this I-V measurement. The low circuit current (I_{SC}) and large open-circuit voltage (V_{OC}) deficiency were believed to be the main reason behind the inability of the device to generate high PCE and FF. The presence of a larger density of charged defects was believed to be the reason behind the poorer current collection efficiency which causes low J_{SC} [23]. Bandgap grading might be used to solve the problem related to poorer current collection efficiency by partially substitute constituent S with Se [24]. Recombination is one reason for the existence of large V_{OC} deficiency [19]. The amount of built-up charges at the opposite ends of a p-n junction reduced by the presence of recombinative process. The decomposition product of the CZTS absorber due to the formation of thick small grains of the absorber layer forms unidentified secondary phases [25]. These unidentified secondary phases with bandgap smaller than absorber layer act as traps and recombination centres which cause large V_{OC} deficiency. Meanwhile, the presence of ZnS secondary phases which has bandgap larger than the absorber layer will narrow the conduction pathways, increasing R_S, and lowering FF of the device [19]. To remove these secondary phases, etchants could be used as one solution [26]–[28]. KCN could be used to remove secondary phases with bandgap smaller than the absorber layer, while HCL could be used to remove secondary phases with bandgap both smaller or larger than the absorber layer.

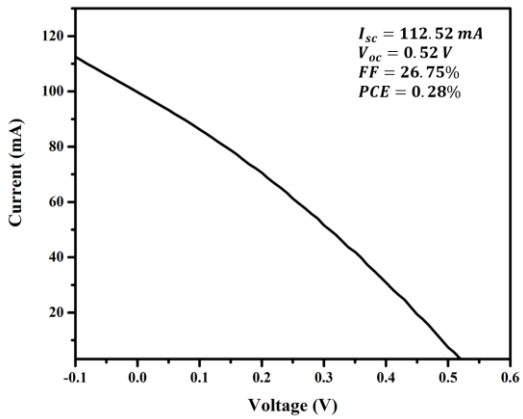

Figure 7. I-V Characteristic of sample A (Zn:Sn = 1:19).

4. CONCLUSION

The semiconductor layers of CZTS-based thin-film solar cells were fabricated under non-vacuum conditions using the spin-coating process. The bandgap energy of the CZTS absorber layer and ZTO buffer layers are ~1.5 eV and ~3.7 eV, respectively. The photovoltaic parameters of the best device, namely sample A, remained low and need further optimization. The measured PCE, FF, J_{SC} and V_{OC} were 0.28%, 26.75%, 112.52 mA, 0.52 V, respectively. However, in

this study, we have been successfully displayed that ZTO is possibly used as an alternative buffer layer for CZTS-based thin-film solar cells using all-solution-non-vacuum produce.

ACKNOWLEDGMENTS

This work was supported by the Program Penelitian Kolaborasi Indonesia, Ministry of Research, Technology and Higher Education, Republic of Indonesia 2019.

REFERENCES

[1] N. Nakayama & K. Ito, "Sprayed films of stannite Cu2ZnSnS 4," Appl. Surf. Sci. **2** (1996) 2–6.
[2] H. Katagiri, N. Sasaguchi, S. Hando, S. Hoshino, J. Ohashi, & T. Yokota, "Preparation and evaluation of Cu2ZnSnS4 thin films by sulfurization of E-B evaporated precursors," Sol. Energy Mater. Sol. Cells **49** (1997) 407–414.
[3] N. Moritake, Y. Fukui, M. Oonuki, K. Tanaka, & H. Uchiki, "Preparation of Cu2 ZnSnS4 thin film current topics in solid state physics solar cells under non-vacuum condition," Phys. Status Solidi C **1236**, 5 (2009) 1233–1236.
[4] S. Lie *et al.,* "Improving Carrier-Transport Properties of CZTS by Mg Incorporation with Spray Pyrolysis," ACS Appl. Mater. Interfaces **11** (2019) 25824–25832.
[5] W. Yang *et al.,* "Molecular Solution Approach To Synthesize Electronic Quality Cu 2 ZnSnS 4 Thin Films," J. Am. Chem. Soc., (2013).
[6] K. Kaur, N. Kumar, & M. Kumar, "Strategic review of interface carrier recombination in earth abundant Cu-Zn-Sn-S-Se solar cells: current challenges and future prospects," J. Mater. Chem. A Mater. energy Sustain. **5** (2017) 3069–3090.
[7] M. Beres, J. Syzdek, K. M. Yu, & S. S. Mao, "Growth behavior of co-electrodeposited CZTS precursor thin films from acidic baths containing tartaric acid," Mater. Chem. Phys. **204** (2018).
[8] J. Paier, M. Marshman, K. Hummer, G. Kresse, I. Gerber, & J. Angyan, "Screened hybrid density functionals applied to solids," J. Chem. Phys. **154709**, no. April (2006).
[9] W. Wang *et al.,* "Device Characteristics of CZTSSe Thin-Film Solar Cells with," Adv. Energy Mater., (2013) 1–5.
[10] J. Li *et al.,* "Solar Energy Materials & Solar Cells 10 % Efficiency Cu 2 ZnSn (S, Se) 4 thin film solar cells fabricated by magnetron sputtering with enlarged depletion region width," Sol. Energy Mater. Sol. Cells **149** (2016) 242–249.
[11] C. Platzer-Bjorkman, C. Frisk, J. Larsen, & T. Ericson, "Reduced interface recombination in Cu2ZnSnS4 solar cells with atomic layer deposition Zn1 − x Sn x O y buffer layers," Appl. Phys. Lett. **243904**, no. November (2015) 1–5.
[12] S. A. Nadi *et al.,* "Postdeposition Annealing Effect on Cu 2 ZnSnS 4 Thin Films Grown at Different Substrate Temperature," Int. J. Photoenergy, (2014) 1–8.
[13] B. Shin, O. Gunawan, Y. Zhu, N. A. Bojarczuk, S. J. Chey, & S. Guha, "Thin film solar cell with 8.4% power conversion efficiency using an earth-abundant Cu 2 ZnSnS 4 absorber," Prog. PHOTOVOLTAICS Res. Appl., no. December 2017 (2013).
[14] S. H. Hadke *et al.,* "Synergistic Effects of Double Cation Substitution in Solution-Processed CZTS Solar Cells with over 10% Efficiency," Adv. Energy Mater. **1802540** (2018) 1–9.
[15] T. K. Todorov, K. B. Reuter, & D. B. Mitzi, "High-Efficiency Solar Cell with Earth-Abundant Liquid-Processed Absorber.pdf," Adv. Energy Mater. **22** (2010).
[16] S. Lie *et al.,* "Improving the charge separation and collection at the buffer/ absorber interface by double-layered Mn-substituted CZTS," Sol. Energy Mater. Sol. Cells **185**, April (2018) 351–358.
[17] X. Cui *et al.,* "Enhanced Heterojunction Interface Quality To Achieve 9.3% Efficient Cd-Free Cu 2 ZnSnS 4 Solar Cells Using Atomic Layer Deposition ZnSnO Buffer Layer," Chem. Mater. **30** (2018) 7860–7871.

[18] I. Repins *et al.,* "Kesterites and Chalcopyrites: A Comparison of Close Cousins Preprint," no. May (2011).
[19] T. J. Huang, X. Yin, G. Qi, & H. Gong, "CZTS-based materials and interfaces and their effects on the performance of thin film solar cells," Phys. Status Solidi RRL **28** (2014) 1–28.
[20] K. Tanaka, M. Oonuki, N. Moritake, & H. Uchiki, "Cu 2 ZnSnS 4 thin film solar cells prepared by non-vacuum processing," Sol. Energy Mater. Sol. Cells **93** (2009) 583–587.
[21] K. Tanaka, Y. Fukui, N. Moritake, & H. Uchiki, "l composition dependence of morphological and optical properties of Cu 2 ZnSnS 4 thin films deposited by sol-gel sulfurization and Cu 2 ZnSnS 4 thin film solar cell efficiency," Sol. Energy Mater. Sol. Cells **95**, 3 (2011) 838–842.
[22] A. Wisitsoraat, A. Tuantranont, E. Comini, G. Sberveglieri, & W. Wlodarski, "Characterization of n-type and p-type semiconductor gas sensors based on NiO x doped TiO 2 thin films," Thin Solid Films **517**, 8 (2009) 2775–2780.
[23] T. J. Pundsack, B. D. Chernomordik, E. S. Aydil, & D. A. Blank, "Excited-State Dynamics in CZTS Nanocrystals," Phys. Chem. Lett., (2013) 2711–2714.
[24] M. Gloeckler & J. R. Sites, "Band-gap grading in Cu (In, Ga) Se 2 solar cells," J. Phys. Chem. **66** (2005) 1891–1894.
[25] S. Siebentritt, "Why are kesterite solar cells not 20 % efficient?," Thin Solid Films **535** (2013) 1–4.
[26] M. Mousel *et al.,* "HCl and Br 2 -MeOH etching of Cu 2 ZnSnSe 4 polycrystalline absorbers," Thin Solid Films **535** (2013) 83–87.
[27] A. Fairbrother, E. Garc, V. Izquierdo-roca, & X. Fontane, "Development of a Selective Chemical Etch To Improve the Conversion Efficiency of Zn-Rich Cu 2 ZnSnS 4 Solar Cells," J. Am. Chem. Soc., (2012) 8018–8021.
[28] M. Mousel *et al.,* "Cu-Rich Precursors Improve Kesterite Solar Cells," Adv. Energy Mater., (2014) 1–6.